Electrochemical treatment of waste solutions containing ferrous sulfate by anodic oxidation using an undivided reactor

J.M. BISANG

Programa de Electroquímica Aplicada e Ingeniería Electroquímica (PRELINE), Facultad de Ingeniería Química (UNL), Santiago del Estero 2829, 3000 Santa Fe, Argentina

Abstract

This paper describes an analysis of the performance of an electrochemical undivided reactor for the recycling of waste solutions containing ferrous sulfate. The effect of oxygen evolution as side anodic reaction on the figures of merit of the reactor is studied. The results suggest that the anode potential must represent a compromise between the increase in space time yield and the increase in the specific energy consumption. Experimental data are correlated with a mathematical treatment based on the stirred tank model.

List of symbols

a_e specific surface area (m^{-1})
b constant in the Tafel equation (V^{-1})
C concentration (mol m^{-3})
E_{SCE} anode potential referred to saturated calomel electrode (V)
E_s specific energy consumption (kWh mol^{-1})
F Faraday constant (C mol^{-1})
h optimal bed depth parallel to the current flow (m)
i current density (A m^{-2})
i_{lim} limiting current density (A m^{-2})
i_s current density of the side reaction (A m^{-2})
I total current (A)
k mass transfer coefficient (m s^{-1})

k_s kinetic constant of the side reaction (A m^{-2})
m exponent in Equation 15
Q charge (C)
t time (s)
V volume of the reactor (m^3)
x fractional conversion
Y parameter given by Equation 18 (C m^{-3})

Greek characters

α constant in Equation 15
β current efficiency
$\Delta\eta$ admitted range of overpotential (V)
v_e charge number of the electrode reaction
ρ space time yield (mol m^{-3} s^{-1})
ρ_s effective electrolyte resistivity (Ω m)

1. Introduction

Many industrial processes produce effluents containing ferrous ions. Examples of waste solutions containing acidic Fe(II) are: (i) pickling of iron and steel where sulphuric and hydrochloric acid are frequently used [1], (ii) processes for coal oxidation [2] or for the destruction of carbonaceous waste [3, 4], (iii) manufacture of printed circuit boards [5] and (iv) acid mine drainage water [6, 7]. For the first three cases the effluent is a concentrated solution of Fe(II), which can be recycled after reoxidation to Fe(III). But acid mine drainage generates an effluent of low Fe(II) concentration, which must be oxidized prior to removal as hydrous ferric oxide at pH higher than 4, as jarosite at lower pH or by selective ionic exchange. Thus, the oxidation of Fe(II) to Fe(III) is a necessary step for the recycling or processing of the solution. Several oxidizing agents are in use [8], such as

oxygen, ozone and chlorine. When oxygen and ozone are used, the reaction produces water and an evaporation step is required. Chlorine as oxidizing agent does not introduce additional water into the solution but there are safety issues. Therefore, the electrochemical oxidation of Fe(II) to Fe(III) represents an alternative method for the treatment of effluents containing Fe(II).

Many authors have performed fundamental kinetic studies for the Fe(III)/Fe(II) couple, as summarized by Heussler [9]. Recently, Ye and Fedkiw [10] studied the kinetics of ferrous oxidation on Pt and Nafion®-coated Pt electrodes in the absence and presence of toluene or benzoic acid. It was concluded that platinum electrodes electrodeposited within a Nafion® film coated onto a glassy carbon substrate were particularly effective in mitigating the effects of contaminants on the oxidation kinetics of Fe(II). Marconi et al. [8] studied the recovery of pickling effluents by electrochemical oxidation of
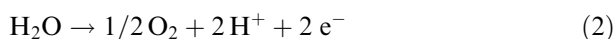
ferrous to ferric chloride using an electrochemical reactor with a three-dimensional graphite felt anode. An anion selective membrane was used as separator to hinder the reduction of the anodically formed Fe(III) at the cathode. Complete oxidation with high current efficiency is reported.

Because the equilibrium potential of the Fe(III)/Fe(II) couple is more negative than those of chlorine and oxygen evolution, the Fe(II) oxidation takes place as sole reaction over a range of potentials but at high potentials gas evolution as anodic side reaction occurs simultaneously. In general, a side reaction is detrimental to the performance of an electrochemical reactor due to the following: (i) a decrease in current efficiency, (ii) contamination of the electrode surface by reaction products, (iii) kinetic coupling with the main reaction, and (iv) in the case of a three-dimensional structure the additional current drained by the side reaction alters the potential distribution in the electrode and reduces the optimum bed thickness parallel to current flow [11]. However, when the side reaction generates a gas, on one hand the effective resistivity of the solution is increased but on the other hand the gas generation acts as a turbulence promoter, thus enhancing the mass transfer to the electrode [12]. Likewise, the gas generation in three dimensional structures can produce channelling in the electrode making some regions inactive or blocking the electrode. Gas generation as side reaction may thus show both beneficial and deleterious effects for the electrochemical reactor.

Likewise, cylindrical electrochemical reactors represent a practical and attractive geometry giving uniform primary current distribution and have been proposed as undivided reactors for indirect electrosynthesis [13]. In this case, the useful species is generated at a large cylindrical electrode, being reconverted only partially at the thin central wire electrode since its area is much smaller. At the same time, at the central electrode, a secondary reaction takes place lowering the current efficiency of the unwanted reconversion. Thus an undivided cell offering an appreciable cell voltage decrease and simplified constructive features can be applied. Therefore, for the electrochemical recovery of waste solutions containing ferrous ions the main anodic reaction is

$$Fe^{2+} \rightarrow Fe^{3+} + e^- \qquad (1)$$

with the side anodic reactions being

$$H_2O \rightarrow 1/2\,O_2 + 2\,H^+ + 2\,e^- \qquad (2)$$

or

$$2\,Cl^- \rightarrow Cl_2 + 2\,e^- \qquad (3)$$

depending on the solution composition. In an undivided cylindrical reactor the inverse of Reaction 1 and also the iron deposition can occur at the cathode, but these reactions can be assumed negligible due to the fact that the ratio between the cathodic and anodic areas is small. Consequently, hydrogen evolution as main cathodic reaction must be expected

$$2\,H^+ + 2\,e^- \rightarrow H_2 \qquad (4)$$

The purpose of the present work is to analyse the anodic oxidation of Fe(II) in an undivided cylindrical electrochemical reactor and to study the effect of oxygen evolution, as the anodic side reaction, on the performance of the reactor in order to discuss criteria for the adoption of the optimal anode potential.

2. Fundamental studies

Prior to the applied studies, the electrochemical behaviour of the Fe(II) oxidation with a rotating disc electrode was analysed. The working electrode was a graphite rotating disc of 6.3×10^{-3} m diameter embedded in a Teflon bell of 34.5×10^{-3} m base diameter. The counter-electrode was a platinum spiral, 140 mm long and 0.7 mm diameter, and as reference a saturated calomel electrode was used. The potentials are referred to this electrode. All experiments were performed at 30 °C under a slow potentiodynamic sweep of 1 mV s^{-1}. The solution was approximately 0.5 M FeSO$_4$ with 0.5 M H$_2$SO$_4$ as supporting electrolyte. The exact Fe(II) concentration was determined by titration against 0.02 M KMnO$_4$ [14]. Sulphuric acid was used as supporting electrolyte instead of hydrochloric acid in order to avoid chlorine evolution as the product of the anodic side reaction (Reaction 3) which can chemically oxidize Fe(II) in an efficient manner. This additional chemical reaction would unnecessarily complicate data interpretation. Likewise, chemical oxidation of Fe(II) by oxygen is known, but this reaction is extremely slow [12] and the amount of Fe(III) chemically produced during the short time of the experiment can be considered negligible.

Figure 1 shows the polarization curves at different angular velocities. Fe(II) oxidation at graphite takes place at limiting current over a large range of potentials, higher than 0.8 V. Taking into account the potential distribution in three-dimensional electrodes, the optimum bed depth parallel to the current flow is given by the following expression [15]:

$$h = \left(\frac{2\Delta\eta}{\rho_s a_e i_{lim}} \right)^{0.5} \qquad (5)$$

Assuming $\Delta\eta = 0.8$ V and typical values for the other parameters of a three-dimensional electrode, such as: $\rho_s = 0.09\ \Omega$ m, $a_e = 3950$ m^{-1}, $i_{lim} = 1819$ A m^{-2} and h is 1.8×10^{-3} m. The limiting current density was calculated for 0.5 M Fe(II) concentration with a mass transfer coefficient taken from Cano and Böhm [16]. Thus, the small value of h restricts the use of three-dimensional
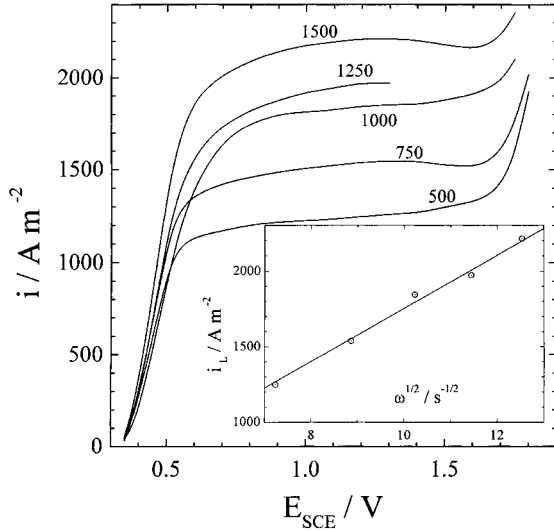
Fig. 1. Current density as a function of the electrode potential for graphite rotating disc electrodes at different angular velocities in rpm. Scan rate: 1 mV s^{-1}. $T = 30$ °C. Electrolyte: 0.5 M H$_2$SO$_4$, C$_{Fe(II)}$ = 0.5 M. Inset: Levich plot.

electrodes for Fe(II) oxidation. A similar conclusion was reached by Marconi et al. [8]. Therefore, for the applied studies a sheet of expanded metal was used as anode. From the slope of the Levich plot, included as an inset in Figure 1, the Fe(II) diffusion coefficient is 4.62×10^{-10} m^2 s^{-1}, which is in reasonable agreement with previous values [10]. Other important properties of the electrolyte are listed in Table 1.

3. Batch electrochemical reactor model

Taking into account Equation 1, for a simple batch reactor the reactant concentration, the fractional conversion and the instantaneous space time yield as a function of time are given by [17]

$$C(t) = C(0) \exp(-ka_e t) \tag{6}$$

$$x(t) = 1 - \exp(-ka_e t) \tag{7}$$

$$\rho(t) = ka_e C(t) \tag{8}$$

In Equations 6 to 8 an electrochemical reaction controlled by mass transfer was assumed.

The charge used by the main and side reactions is

$$dQ = a_e V(v_e F k C(t) + i_s) dt \tag{9}$$

Table 1. Properties of the electrolyte

Density/kg m^{-3}	1.097×10^3
Dynamic viscosity/kg m^{-1} s^{-1}	1.13×10^{-3}
Kinematic viscosity/m^2 s^{-1}	1.03×10^{-6}
Diffusion coefficient/m^2 s^{-1}	4.62×10^{-10}
Schmidt number	2229
Resistivity/Ω m	5.87×10^{-2}

Introducing Equation 6 into Equation 9 and integrating gives

$$\frac{Q}{V} = v_e F C(0)(1 - \exp(-ka_e t)) + a_e i_s t \tag{10}$$

Combining Equations 7 and 10 yields

$$\frac{Q}{V} = v_e F C(0)x + \frac{i_s}{k}\ln(1 - x) \tag{11}$$

which gives, in an implicit manner, the fractional conversion as a function of both the charge used in the reactor and the current density of the side reaction, which depend on the applied potential to the working electrode.

Likewise, the mean value of the space time yield during the time t of the experiment is given by

$$\rho_{mean} = \frac{1}{t} \int_0^t \rho(t) dt \tag{12}$$

Introducing Equations 8 and 6 into Equation 12 and integrating yields

$$\rho_{mean} = \frac{C(0)x(t)}{t} \tag{13}$$

Combining Equations 10 and 13 and rearranging gives

$$\frac{Q}{V} = v_e F C(0)\left[1 - \exp\left(-\frac{ka_e C(0)x(t)}{\rho_{mean}}\right)\right] + \frac{a_e i_s C(0)x(t)}{\rho_{mean}} \tag{14}$$

which gives the effect of the side reaction on the mean value of the space time yield for a given charge used in the reactor.

At lower potentials the rate of the side reaction is small and the second term on the right hand side in Equations 11 and 14 can be neglected. However, at higher potentials i_s is appreciable and the combined effect of natural convection and bubble-induced convection produced by the side reaction must be taken into account to calculate the mass transfer coefficient. Additionally, the bubble-induced convection due to the gas generated at the counterelectrode must also be considered. However, one effect usually predominates in the mass-transfer process and, therefore, Newman [18] recommends that the mass transfer coefficient for an individual mode of operation must be determined separately and the higher value must be applied. Therefore, at high potentials the effect of the bubble-induced convection produced by the oxygen evolution at the working electrode predominates. In view of the complex nature of mass transfer at gas evolving electrodes it is difficult to propose a general mass transfer correlation which can be used in the design and

operation of gas evolving electrochemical reactors. However, the following empirical relationship can be accepted for k [19]

$$k = \alpha i_s^m \tag{15}$$

where the exponent m is a number lower than one. Likewise, a Tafel equation can be adopted for i_s

$$i_s = k_s \exp(bE) \tag{16}$$

Combining Equations 11, 15 and 16 and rearranging yields

$$\ln(Y) = \ln\left(\frac{k_s^{1-m}}{\alpha}\right) + b(1-m)E \tag{17}$$

where

$$Y = \frac{v_e FC(0)x - Q/V}{\ln(1-x)} \tag{18}$$

4. Experimental details

The experiments were performed in an undivided reactor (70 mm int. dia. × 90 mm high) with cylindrical concentric electrodes. The reactor was thermostated by a heating jacket. The working electrode was a cylindrical sheet of expanded titanium coated with platinum (51 mm dia. × 24 mm high) and was arranged in the reactor with the long diagonal vertical. Table 2 gives the geometrical characteristics of the expanded metal (micromesh). The counterelectrode was a Pt wire (0.7 mm dia. × 50 mm long). Therefore, the anode area was approximately sixty times the cathode area. As reference a saturated calomel electrode was used and the potentials are referred to this electrode. All experiments were performed at 30 °C under potentiostatic control up to a charge of 2679 C. The solution was approximately 0.5 M $FeSO_4$ and 0.5 M H_2SO_4 as supporting electrolyte and the solution volume in each experiment was 0.25 dm^3. The initial and final Fe(II) concentrations were determined by titration against 0.02 M $KMnO_4$ [14]. During the experiment small iron dendrites were observed at the cathode, which broke away from the electrode, aided by the abundant hydrogen evolution, and redisolved in the acid solution. At the end of the experiment the cathode was left in the solution in order

Table 2. Geometrical characteristics of the expanded metal

Long diagonal/mm	6
Short diagonal/mm	3
Long mesh aperture/mm	4.6
Short mesh aperture/mm	1.6
Thickness/mm	0.5
Apparent thickness/mm	1.2
Strand width/mm	0.7
Surface area per unit volume of electrode/m^{-1}	1288

to allow dissolution of the small amount of residual deposited iron. Iron is dissolved in the acid solution with generation of hydrogen

$$Fe + 2H^+ \rightarrow Fe^{2+} + H_2 \tag{19}$$

and also by the Fe(III) ions

$$Fe + 2Fe^{3+} \rightarrow 3Fe^{2+} \tag{20}$$

However, because the amount of deposited iron is small the concentration change of Fe(II) and Fe(III) due to Equations 19 and 20 is negligible and has not been considered in the mathematical model. Therefore, the difference between the initial and final Fe(II) concentration gives the amount of Fe(II) oxidized to Fe(III).

5. Results and discussion

Figure 2 shows the current efficiency as a function of applied potential and also includes the polarization curve for oxygen evolution, obtained with the same reactor and a 0.5 M H_2SO_4 solution. Comparing Figures 1 and 2 it can be observed that, at a platinum electrode, the onset of oxygen evolution takes place at a potential lower than at graphite electrodes. Therefore, at a platinum anode the range of overpotential in Equation 5 is low, which further restricts the thickness of the electrode parallel to current flow. Figure 2 also shows that for potentials lower than 1.2 V the current efficiency is high, between 95–100%, which demonstrates that the predominant cathodic reaction is hydrogen evolution. For potentials higher than 1.2 V oxygen evolution, as side anodic reaction, begins and the current efficiency decreases as expected.

The points in Figure 3 correspond to experimental values of the fractional conversion as a function of
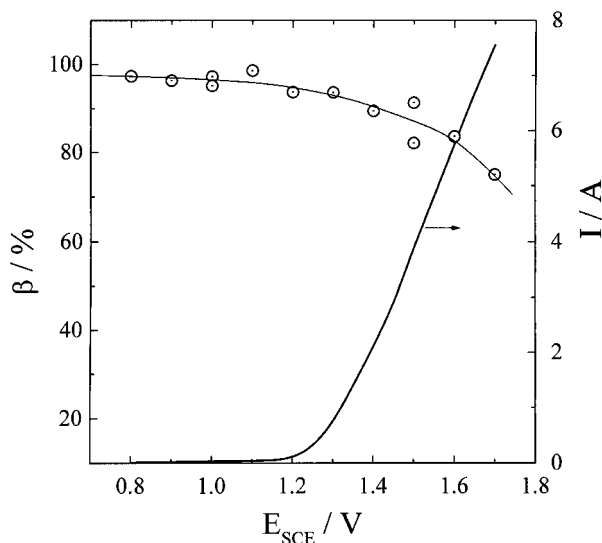
Fig. 2. Current efficiency as a function of the applied potential for the batch reactor. Thick line: polarization curve of oxygen evolution from 0.5 M H_2SO_4, $T = 30$ °C.
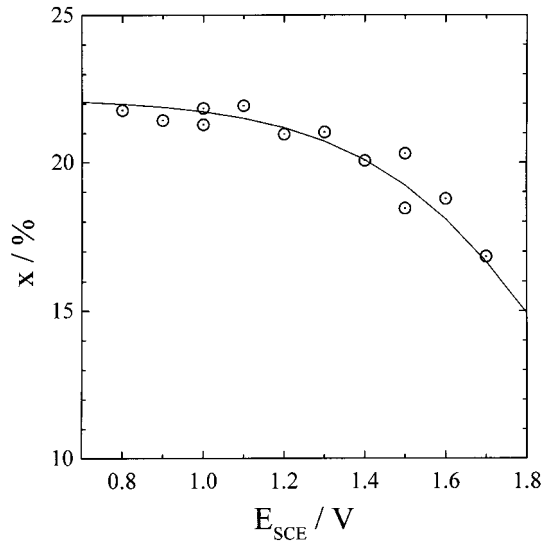
Fig. 3. Conversion as a function of the applied potential for the batch reactor. Full line: Equation 11 evaluated with the fitting parameters of Figure 4.

Fig. 5. Duration of the experiment as a function of the applied potential for the batch reactor. Total charge 2679 C.

applied potential. At potentials lower than 1.2 V Fe(II) oxidation takes place as sole reaction and, due to the fact that it is controlled by mass transfer, the fractional conversion is a constant. At high applied potential oxygen evolution as anodic side reaction begins and affects the fractional conversion. On one hand an increase in the potential produces an increase in oxygen generation, which promotes localized turbulence near the electrode surface thus enhancing the mass transfer of Fe(II) to the electrode. Thus, the fractional conversion is increased. On the other hand oxygen evolution reduces the time necessary to pass 2679 C and the fractional conversion decreases. The second factor predominates over the first and a small decrease in fractional conversion with applied potential is observed. In order to verify the ability of the model to correlate the experi-
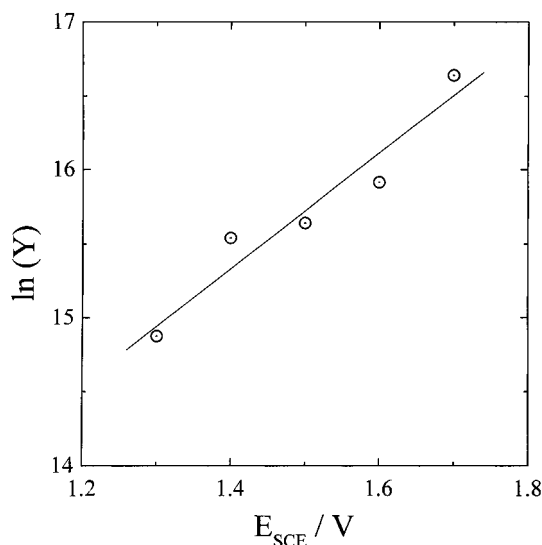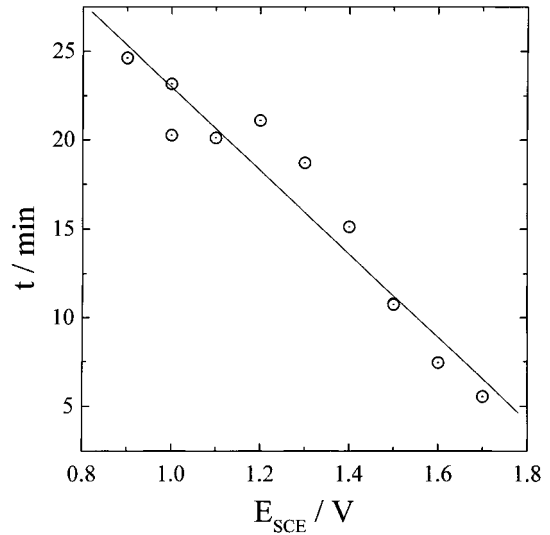
mental results, the data of Figure 3 are replotted in Figure 4 in logarithmic form according to Equations 17 and 18. The line of Figure 4 fits the experimental data with a standard deviation of 0.195, which represents a reasonable agreement in view of the difficulties of calculating the mass transfer coefficient. The full line in Figure 3 corresponds to Equation 11 evaluated with the fitting parameters of Figure 4. From the slope and the intercept of the line of Figure 4 and assuming common kinetic constants for oxygen evolution such as $b = 21$ V^{-1} and $k_s = 1 \times 10^{-12}$ A m^{-2} gives $m = 0.81$. This value of m lies near the upper point of the wide range of experimental values compiled by Vogt [19].

Figure 5 shows the required time to pass a charge of 2679 C as a function of potential. The time, duration of the experiment, is drastically reduced when the applied

Fig. 4. Linearized representation of the fractional conversion data according to Equations 17 and 18.
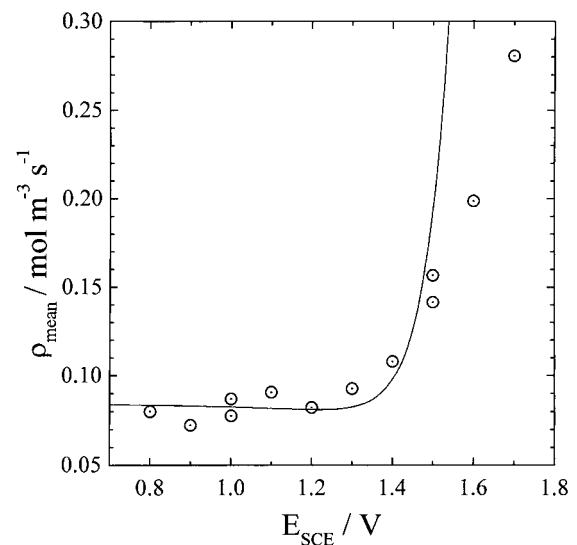

Fig. 6. Mean space time yield as a function of the applied potential for the batch reactor. Full line: prediction of Equation 14 with the fitting parameter of Figure 4.
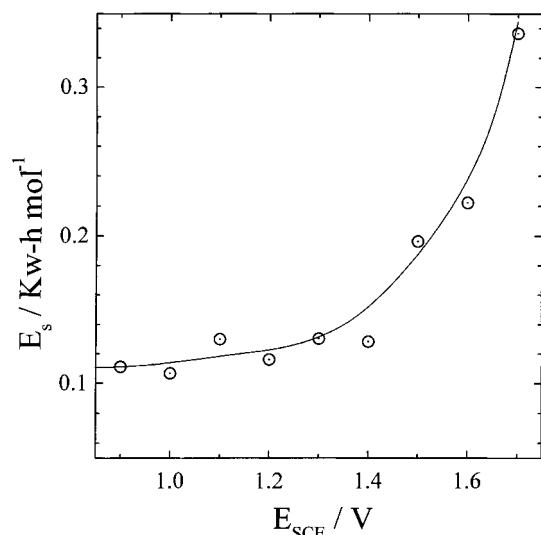
Fig. 7. Specific energy consumption as a function of the applied potential for the batch reactor.

potential increases despite the fractional conversion (Figure 3) being rather similar in all cases.

Figure 6 shows the mean value of the space time yield as a function of applied potential. For potentials lower than 1.2 V the space time yield is practically constant. However, ρ_{mean} increases markedly with increase in potential because the oxygen evolution acts as a turbulence promoter. Thus for a given production the size of the reactor is reduced. The full line in Figure 6 corresponds to Equation 14 evaluated with the fitting parameters of Figure 4. The numerical calculations demonstrate that the results of Equation 14 are very sensitive to the values of the kinetic constants of the side reaction, k_s and b. Therefore, Equation 14 may be used for the estimation of the mean value of the space time yield but special attention must be paid to the choice of kinetic constants for the side reaction.

Figure 7 shows the specific energy consumption as a function of applied potential. E_s increases with increase in potential. Comparing Figures 6 and 7 it can be concluded that oxygen evolution as side anodic reaction presents both beneficial and detrimental aspects. Thus, when the applied potential increases both the space time yield and the specific energy consumption also increase and the choice of potential depends on a compromise between the initial investment cost and the energy cost.

Conclusions

The following conclusions may be drawn:
(i) It was demonstrated that the regeneration of waste solutions containing Fe(II) may be performed in an efficient manner with an undivided electrochemical reactor providing a small ratio between the cathodic and the anodic areas. The absence of a separator reduces the cell voltage and the construction features are simplified.

(ii) The side reactions cannot be considered *a priori* as detrimental for the performance of electrochemical reactors; in many important industrial cases the side reactions can be beneficial, such as in the present study case.
(iii) The mathematical treatment based on the stirred tank model has proved appropriate for correlation of the experimental results when side reactions, evolving a gas as a product, take place simultaneously with the main reaction at the electrode.
(iv) The applied potential of the working electrode must be adopted from an economic point of view taking into account the initial investment costs and the energy price.

References

1. P.N. Burkard, *in* 'Modern Electroplating', edited by F.A. Lowenheim (J. Wiley & Sons, New York, 1974), chapter 23, p. 583.
2. G. Kreysa and W. Kochanek, *J. Electrochem. Soc.* **132** (1985) 2084.
3. R.L. Clarke, *in* 'Electrochemistry for a Cleaner Environment', edited by D. Genders and N. Weinberg (The Electrosynthesis Company, New York, 1992), chapter 13, p. 271.
4. K. Rajeshwar and J. Ibanez, 'Environmental Electrochemistry' (Academic Press, New York, 1997), chapter 5, p. 401.
5. D. Pletcher and F.C. Walsh, 'Industrial Electrochemistry' (Chapman & Hall, London, 1993), chapter 9, p. 471.
6. G.B. Adams, R.P. Hollandsworth and D.N. Bennion, *J. Electrochem. Soc.* **122** (1975) 1043.
7. G.B. Adams, R.P. Hollandsworth and D.N. Bennion, *AIChE Symposium Series* **73** (166) (1977) 99.
8. P.E. Marconi, V. Meunier and N. Vatistas, *J. Appl. Electrochem.* **26** (1996) 693.
9. K.E. Heusler, *in* 'Encyclopedia of Electrochemistry of the Elements', Vol. IX, Part A, edited by A.J. Bard, (Marcel Dekker, New York, 1982).
10. J.-H. Ye and P.S. Fedkiw, *J. Electrochem. Soc.* **141** (1996) 1483.
11. J.M. Bisang, *J. Appl. Electrochem.* **26** (1996) 135.
12. M.F. El-Sherbiny, A.A. Zatout, M. Hussien, G.H. Sedahmed, *J. Appl. Electrochem.* **21** (1991) 537.
13. A.J. Bellamy and B.R. Simpson, *Chem. Ind.* (London) (1981) 328.
14. I.M. Kolthoff, E.B. Sandell, E.J. Meehan and S. Bruckenstein, 'Quantitative Chemical Analysis', 4th edn (MacMillan, New York, 1969).
15. G. Kreysa, *DECHEMA Monographs* **94** (1983) 123.
16. J. Cano and U. Böhm, *Chem. Eng. Sci.* **32** (1977) 213.
17. F.C. Walsh, 'A First Course in Electrochemical Engineering' (Alresford Press, Alresford, 1993), chapter 6, p. 175.
18. J.S. Newman, 'Electrochemical Systems' (Prentice Hall, Englewood Cliffs, NJ, 1973), chapter 17, p. 330.
19. H. Vogt, *in* 'Comprehensive Treatise of Electrochemistry', Vol. 6, edited by E. Yeager, J.O'M. Bockris, B.E. Conway and S. Sarangapani (Plenum Press, New York, 1983), chapter 7, p. 456.